THE INSTITUTE OF SPACE AND ASTRONAUTICAL SCIENCE
YOSHINODAI, SAGAMIHARA, KANAGAWA 229

ISAS RESEARCH NOTE

ISAS RN 567

Analog Alignment Control for the TENKO-100 DL Interferometer

E.G. Heflin , N. Kawashima

March, 1995

Analog Alignment Control for the TENKO-100 DL Interferometer

E.G. Heflin[1], N. Kawashima
The Institute of Space and Astronautical Science
Yoshinodai Sagamihara, Kanagawa 229 Japan

1. Abstract

This paper discusses the structure and implementation of an analog alignment control system for delay-line (DL) interferometers. The goal of the system is to reduce the instabilities from large transient seismic noises, such as nearby passing cars or trucks, and diminish the instabilities from the cumulative effects of background seismic noises which result in the gradual degradation of the interferometer sensisitivity. The system is based on feedback of reflected laser light signals detected with quadrant type photodiodes from each of the five main optical components of the interferometer, i.e. four DL mirrors (two near and two far), and one beamsplitter. The alignment system is new in that it combines the direct use of the main interferometer DL laser light for feedback control of each far mirror and the beamsplitter for a relative reference with the use of an external laser to provide an absolute reference for control of each near mirror. The system was implemented and tested on the 100 m DL interferometer at ISAS, TENKO-100. The analog feedback control demonstrates excellent stability, with standalone operation of more then one hour during daytime (noisy) operation, improved reduction of noise between 22 to 9 dB in the 1 to 30 Hz range, and extended operating times during the day (~ 6 min) and night (~ 25 min).

2. Introduction

The increase in sensitivities for interferometric gravitational wave detectors over the past two decades has been quite impressive, e.g. from $h = 10^{-17}\sqrt{\text{Hz}}/\text{Hz}$ [Weiss] to $h = 5 \times 10^{-20}\sqrt{\text{Hz}}/\text{Hz}$ [CalTech]. With the same rate of progress, it can be reasonably expected that such detectors will attain sensitivities in the range of the signals from near astrophysical sources within the next decade. However, without the ability to retain such sensitivities over long periods of time, i.e.> 1 hr, these advances are meaningless for experiments designed to search for gravitational-wave signals.

To date, the longest recorded high sensitivity run is that by TENKO-10 of 5 hrs and 50 min in 1989 with $h < 2 \times 10^{-18}\sqrt{\text{Hz}}/\text{Hz}$ TENKO-10. Most detectors experience their longest periods of sensitive operation during the relatively "quiet" times, e.g. through the night, and their shortest periods during "noisy" operating times, e.g. through the day. In fact, operation during these noisy periods yields important information about the noises at problem and their sources. Two acute problems during these noisy operational periods are, firstly, the sudden break in locking of sensitivity which is often correlated to large transient seismic noise such as a nearby passing car or truck, and, secondly, the gradual degradation in sensitivity due to the cumulative effects of background seismic noises. Both problems can be solved through proper alignment of the main interferometer laser beam and seismic control of the interferometer optical components, i.e. the four DL mirrors and the beamsplitter.

3. The Alignment System

The reduction of the transient and cumulative seismic noises is performed by aligning the four DL mirrors (two near and two far) and the beam splitter to the main interferometer laser beam. Figure 1 shows the basic system setup, while Figure 2 shows the system flow of information. The system can be divided into three basic basic areas: (*i*) noise signal detection for each optical component from a laser beam spot and photodiode, (*ii*) noise signal processing by filtering and gain control, (*iii*) signal feedback into the local controls of the coil actuators on each optical component. The main optical components controlled by the system are pendular mounted and of two similar types: mirrors (four) and beam splitter (one). Table 1 shows a breakdown of the significant features for these two types of optical components.

The system feedback is based on seismic signals obtained from the five optical components above using quadrant photodiodes with laser beam spots. In the linear regime, the feedback of the signals works on the principle that small rotations of a cylindrically symmetric mirror about its transverse axis, $\Delta\theta_R$ and $\Delta\theta_P$, produce large linear deviations in the transverse positions, x-axis and y-axis.

[1] Visiting Research Associate with NSF/JSPS Fellowship

Element	D/W/L [cm/cm/cm]	M [kg]	f_{res} [Hz]
Near/FarMirror	35.0/8.0/55	22	0.7
BeamSplitter	16.0/2.5/25	3	1

Table 1: The Main Optical Components
The main optical components for feedback control in the alignment system are: the near and far mirrors in each baseline of the DL interferometer (2), and the beamsplitter. Here D is the diameter, W the width, L the suspension length, and M the mass. Although there are geometrical differences, the beamsplitter can be thought of as a scaled down version of the mirrors.

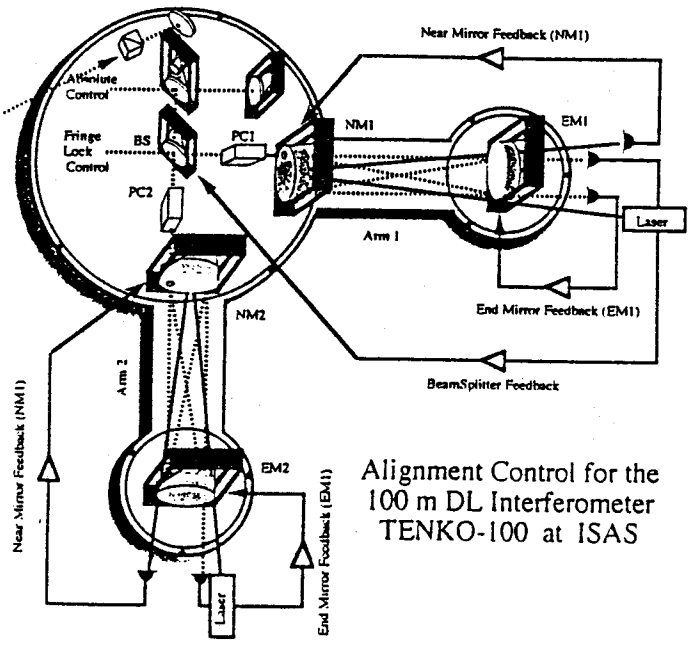

Alignment Control for the 100 m DL Interferometer TENKO-100 at ISAS

Fig. 1.— The Alignment System.
The basic alignment system consists of an external laser beam with a photodiode, a residual DL beam with a photodiode, and analog feedback control for the two mirrors in each baseline of the interferometer. In addition, the beamsplitter is controlled through the signal from the first residual DL beam ,on the "split end" of the interferometer, with a photodiode.

3.1. Noises and Mirror Movements

Figure 3 shows the two basic degrees of freedom important to the pendular motions for the induced seismic noises in the mirrors and beamsplitter. Rotation around the vertical axis (y-axis) corresponds to the "roll" (R) of the mirror, while rotation around the horizontal axis (x-axis) corresponds to the "pitch" (P). Since the two degrees of freedom are orthogonal, they are not correlated and good choices of parameters to describe the transverse rotational motions of the mirrors and beamsplitter.

The alignment system uses reflected light coupled to the long baseline of the interferometer (100 m) in order to "magnify" the small rotational movements of the mirror into large displacements in the transverse x and y-axis observed by the photodiodes.

3.2. Signals

The large linear deviations in the transverse positions along the x-axis and y-axis are detected with sensitive quadrant photodiodes shown in Figure 4. The photodiodes used are Hamamatsu S1406-4 with a quadrant face of 2.4 mm × 2.4 mm and light sensitivity of 320 to 1060 nm. The combination of the output signals is performed by the pre-amplifier circuit shown in Figure 5 to give a voltage proportional x and y positions, allows for high precision feedback control of the reflecting mirror. Note that the signals from the reflected light come from two different sources (ref. Figure 1): (1) the first beam spot of the main DL (Ar laser) in the "split end" baseline of the interferometer for control of the beamsplitter as well as another similar spot from the main DL for relative control of the DL far mirror and (2) an external HeNe laser beam for absolute control of the near mirror.

Typical signals from the quadrant photodiodes are shown in Figure 6 for the time domain and in (a) of Figure 14 for the frequency domain. Note the presence of low frequency noise in the FFT spectrum for a typical photodiode signal. This low frequency noise is correlated to local seismic activity of passing cars and trucks during the day and is evidenced from the time domain output of a typical photodiode.

3.3. Feedback

The feedback for the alignment system consists of 10 different channels corresponding to the x and y-axis of each photodiode for the five different optical components. The feedback circuit for a single chan-

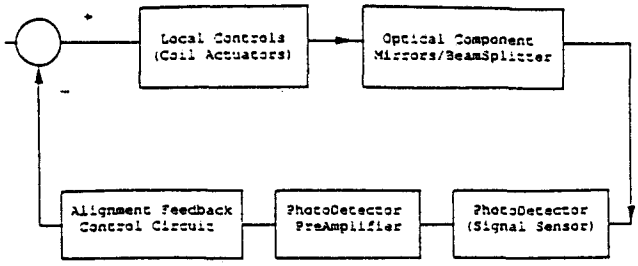

Fig. 2.— The Alignment System Blocks.
The basic alignment system block diagram includes the detection of the reflected light signal by the photodiode, signal processing, and final feedback control to the optical component actuators (mounted coils).

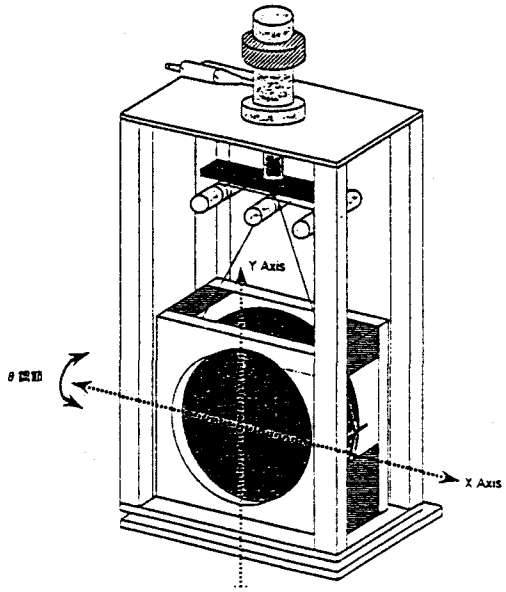

Fig. 3.— The Mirror Motions
The motions for the mirror (and beamsplitter) due to seismic noises can be reduced to the motions around the two transverse axis of the detector. Since the optical components are mounted as pendula by wire around the circumference, it is expected that pitch should be slightly more dynamic than the roll.

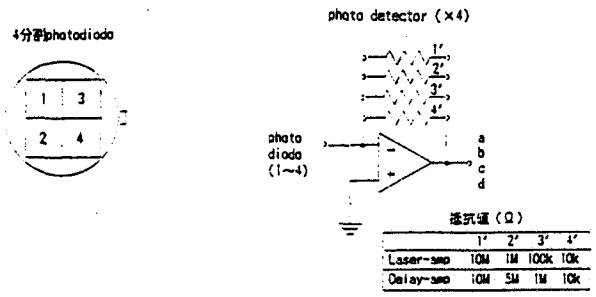

Fig. 4.— The Photodiode.
The photodiode is a quadrant type with output of a voltage from each of the different quadrants as shown. These voltages are amplified and added or subtracted to yield signals corresponding to the x and y axis.

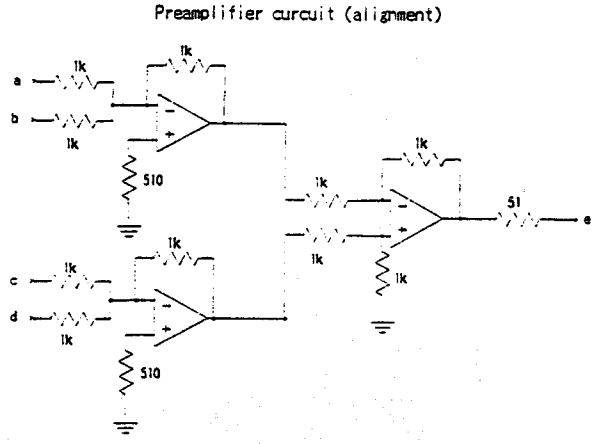

Fig. 5.— The Pre-Amplifier Circuit.
Each of the four voltages from the different quadrants of the photodiode are combined with the above pre-amplifier circuit to give a proportional voltage to the position of the beam spot on the photodiode. These voltages correspond to the x and y positions according to $V_x = [(V_4 + V_3) - (V_2 + V_1)]$ and $V_y = [(V_4 + V_1) - (V_2 + V_3)]$. Note the variable gain of the pre-amplifier to compensate for differences between the DL beam spot signal and the external HeNe beam spot signal.

nel is shown in Figure 7 and its response is shown Figure 8.

3.4. Implementation

The implementation of the alignment system is based on the linear relationship between small angular variations of the optical components due to seismic noises and the photodiode response. For small angular variations, the transformation between the actuator (coil mount) input signals of the mirrors and beamsplitter, R (V_r) and P (V_p), and the photodiode signals from the reflected light beam spots, x (V_x) and y (V_y), is given by the following,

$$\begin{pmatrix} X \\ Y \end{pmatrix} = \begin{bmatrix} m_{X_r} & m_{X_p} \\ m_{Y_r} & m_{Y_p} \end{bmatrix} \begin{pmatrix} R \\ P \end{pmatrix} + \begin{bmatrix} b_{X_r} & b_{X_p} \\ b_{Y_r} & b_{Y_p} \end{bmatrix}$$

Here, the slopes, m, and intercepts, b, can be determined by "sweeping" the local control for the optical component over its dynamic range along both the x-axis (R) and the y-axis (P) of the photodiode, as shown in Figure 9.

A breakdown of the basic step performed in implementing the system is as follows:

(1) photodiode Calibration - Each photodiode is "swept" in x and y to set pre-amplifier gain so that the dynamic range is roughly $\pm$ 50mV. Alignment of the x and y-axis with respect to the X and Y-axis of the optical component is also performed (if the R and P motions of the optical component are orthogonal, any cross correlation in this sweep would indicate a simple rotation of the x and y-axis between the photodiode and the optical component). Finally, the laser beam spot is placed at the center of the photodiode corresponding to the "origin".

(2) Feedback Parameter Optimization - Each channel of the optical component is checked separately for proper phase, frequency, and gain response. This check is performed by maximizing the noise reduction in the time variation response and the power spectrum of the photodiode.

(3) Feedback Control - All 10 channels of the alignment system are fedback and the closed system response is monitored with respect to both time variation response and power spectrum.

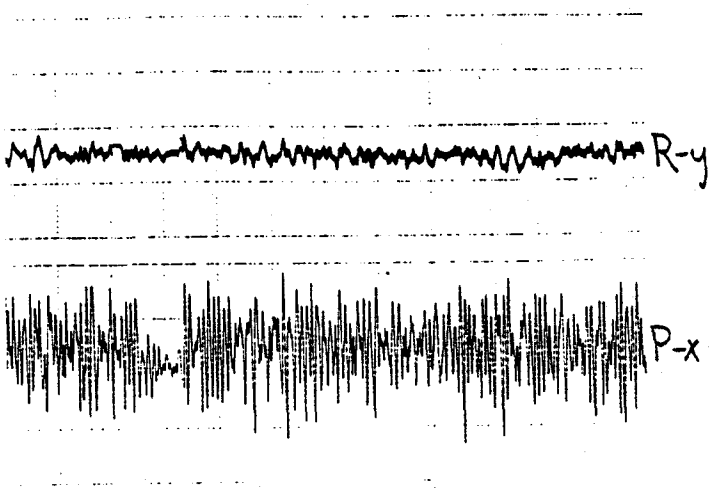

Fig. 6.— Photodiode Signal
The variation spectrum in the time domain for a typical output from a photodiode is shown on top for x (R) and on the bottom for y (P). The most dynamic signal, largest variation, corresponds to the y of the photodiode or the P motion of the corresponding mirror. Notice the cumulative effect of the passage of cars and trucks with the low frequency time variations of the photodiode signal. The time axis is 1 cm $\equiv$ 12 s and the amplitude axis 1 cm $\equiv$ 10 mV.

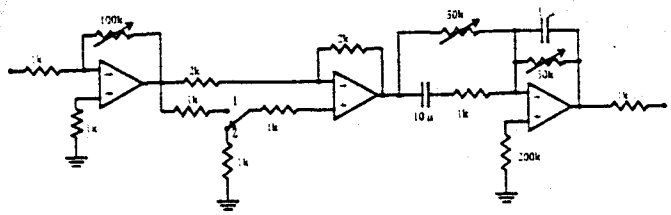

Fig. 7.— The Feedback Circuit.
The feedback circuit for each of the x and y-axis of the photodiode in the alignment system is shown. Each of the five optical components has two feedback circuits corresponding to the two axis of the photodiode (or two degrees of rotational freedom for the optical component).

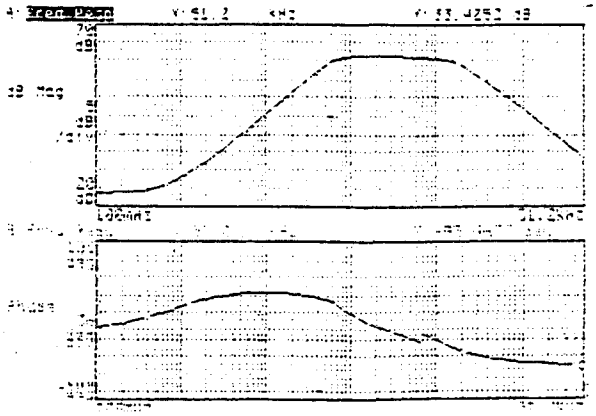

Fig. 8.— The Feedback Response.
A typical Bode diagram for the feedback circuit is shown with gain and phase response. Note the band-pass response in the diagram.

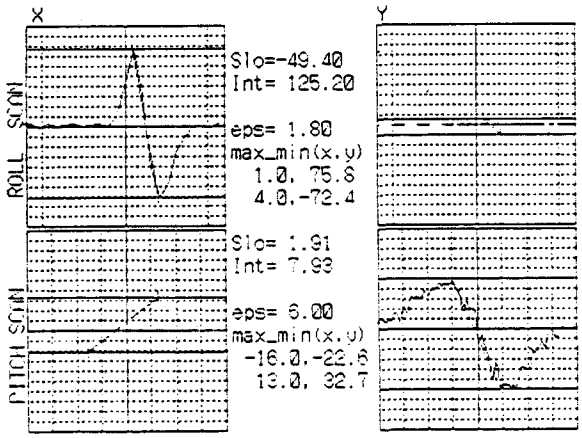

Fig. 9.— Laser Beam Spot-Photodiode Sweep.
The local control of the mirror or beamsplitter can be varied giving rise to changes in the position of the laser beam spot (reflected from the mirror) on the photodiode. By varying the R and P of the optical component, separately, the correlation between the corresponding x and y-axis of the photodiode as well as the proportionally constant, slope of m, and offset, intercepts of b.

4. Theory

The objective in alignment control is to align the main interferometer laser beam to the optical components of the interferometer system, e.g. the near and far mirror in each baseline of the interferometer as well as the beamsplitter. For the two degrees of rotational freedom of the optical components in the main interferometer, this objective can be translated into the following three stability conditions:

(1) $\vec{b_0} \bullet \hat{j} = \sqrt{2}/2$ - The beamsplitter must be $\pi/2$ to the direction of the main laser beam.

(1) $\vec{m_2} \bullet \hat{j} = 1$ - The near mirror must be perpendicular to the direction of an external laser beam.

(2) $\vec{m_2} \bullet \vec{m_1} = -1$ - The end mirror must be perpendicular to the near mirror at all times.

The first condition provides relative referential control for the beamsplitter with respect to the main laser interferometer. The second condition provides absolute referential control for each baseline of delay-line interferometer through the near mirror, while the third provides relative control for each baseline of the delay-line interferometer through the far mirror. These conditions are met by implementing the alignment feedback control according to the three step process outlined above. To better understand the underlying foundation for linear alignment control, it will be useful to derive the basic between the small rotational motions of main optical components and the response of the photodiode signals, in addition to discussing the linear nature of the feedback control.

4.1. Near Mirror and Beamsplitter

In deriving the formula for small angle rotations of the near mirror and beamsplitter, it is assumed that the laser light is reflected from center of the optical component and that the corresponding photodiode is initially centered and aligned with its face perpendicular to the reflected beam. As it turns out, excluding these assumptions will not affect the final results presented here, only the complexity in arriving at them. Shown in Figure 10 is the cross-sectional view of the reflecting mirror (similar scenario for the beamsplitter) in its original position specified by $(\vec{r_i}, \theta_i, \phi_i; \vec{r_r}, \theta_r, \phi_r)$ and, after a rotation of $\Delta\theta$ about the y-axis specified by $(\vec{r_i}', theta_i', \phi_i'; \vec{r_r}', theta_r', \phi_r')$.

The path of the original laser beam (initial state) is noted $\vec{r_i}$ for the incident beam and $\vec{r_o}$ for the reflected beam, while the path of the perturbed laser beam (final state) is noted with primes according to $\vec{r_i}'$ for the incident beam and $\vec{r_o}'$ for the reflected beam.

$$\begin{aligned}
\vec{r_i} &= r_0\left[\hat{\imath}sin\theta_i cos\phi_i + \hat{\jmath}sin\theta_i sin\phi_i + \hat{k}cos\theta_i\right] \\
\vec{r_r} &= r_0\left[\hat{\imath}sin\theta_r cos\phi_r + \hat{\jmath}sin\theta_i sin\phi_i + \hat{r}cos\theta_r\right] \\
&= r_0\left[-\hat{\imath}sin\theta_i cos\phi_i - \hat{\jmath}sin\theta_i sin\phi_i + \hat{k}cos\theta_i\right] \\
\vec{r_i}' &= r_0\left[\hat{\imath}'sin\theta_i' cos\phi_i' + \hat{\jmath}'sin\theta_i' sin\phi_i' + \hat{k}'cos\theta_i'\right] \\
\vec{r_r}' &= r_0\left[\hat{\imath}'sin\theta_r' cos\phi_r' + \hat{\jmath}'sin\theta_r' sin\phi_r' + \hat{k}'cos\theta_r'\right] \\
&= r_0\left[-\hat{\imath}'sin\theta_i' cos\phi_i' - \hat{\jmath}'sin\theta_i' sin\phi_i' + \hat{k}'cos\theta_i'\right]
\end{aligned}$$

Reinterpreting the movement of the mirror as a change in the axis of symmetry between the original beam and the perturbed beam, i.e. a change in the basis vectors of the system due to the simple rotation about y by $\Delta\theta$

$$\begin{pmatrix} \hat{\imath}' \\ \hat{\jmath}' \\ \hat{k}' \end{pmatrix} = \begin{bmatrix} cos\Delta\theta & 0 & sin\Delta\theta \\ 0 & 1 & 0 \\ -sin\Delta\theta & 0 & cos\Delta\theta \end{bmatrix} \begin{pmatrix} \hat{\imath} \\ \hat{\jmath} \\ \hat{k} \end{pmatrix}$$

Since one is interested in a relationship which expresses the change in displacement observed at the photodiode due to the angular perturbation and the original position of the beam, the following relations defining the reflection symmetries of the system,

(1) $\theta_r = \theta_i$ and $\theta_r' = \theta_i'$ - The angle with respect to the transverse axis is constant, in the given basis vector set, for the center of the mirror.

(2) $\phi_i = \pi + \phi_r$ and $\phi_i' = \pi + \phi_r'$ - The mirror center, the incident and the reflected ray all define a plane.

(3) $|\vec{r_i}| = |\vec{r_r}| = |\vec{r_i}'| = |\vec{r_r}'| = z_0/cos\theta_i = r_0$ - The laser source and photodiode are always normal to emitted or received laser beam with $sin\theta_i \approx \theta_i$.

are useful in deriving the relationships necessary to eliminate the primed, $'$, variables, in the following

$$\begin{aligned}
\hat{\imath}' \cdot \vec{r_i}' &= r_0 sin\theta_i' cos\phi_i' = \hat{\imath}' \cdot \vec{r_i} \\
&= r_0\left[cos\Delta\theta sin\theta_i cos\phi_i + sin\Delta\theta cos\theta_i\right] \\
\hat{\jmath}' \cdot \vec{r_i}' &= r_0 sin\theta_i' sin\phi_i' = \hat{\jmath}' \cdot \vec{r_i} \\
&= r_0 sin\theta_i sin\phi_i \\
\hat{k}' \cdot \vec{r_i}' &= r_0 cos\theta_i' = \hat{k}' \cdot \vec{r_i} \\
&= r_0[-sin\Delta\theta sin\theta_i cos\phi_i + cos\Delta\theta cos\theta_i]
\end{aligned}$$

The difference, $\Delta\vec{r_r}$ between the original reflected beam, $\vec{r_r}'$, and the perturbed reflected beam, $\vec{r_r}$, gives

$$\begin{aligned}
\Delta\vec{r}_{r-R} &= [\vec{r_r}' - \vec{r_r}|_{Rrot} \\
&= r_0[((cos^2\Delta\theta - sin^2\Delta\theta - 1)sin\theta_i cos\phi_i \\
&\quad +2cos\theta_i cos\Delta\theta sin\Delta\theta)\hat{\imath} \\
&\quad +((cos^2\Delta\theta - sin^2\Delta\theta - 1)cos\theta_i \\
&\quad +2sin\theta_i cos\phi_i cos\Delta\theta sin\Delta\theta)\hat{k}] \\
&\approx z_0[-(2\Delta\theta)\hat{\imath} \\
&\quad +(2tan\theta_i cos\phi_i\Delta\theta)\hat{k}] \\
&\approx -2z_0\Delta\theta\hat{\imath}
\end{aligned}$$

Here, $cos\Delta\theta \approx 1$, $sin\Delta\theta \approx \Delta\theta$ and $sin\theta_i \approx 0$.

The analogous result is obtained from rotations about the x-axis, as symmetry would dictate, in the form

$$\begin{aligned}
\Delta\vec{r}_{r-P} &= [\vec{r_r}' - \vec{r_r}|_{Prot} \\
&= r_0[((cos^2\Delta\theta - sin^2\Delta\theta - 1)sin\theta_i sin\phi_i \\
&\quad +2cos\theta_i cos\Delta\theta sin\Delta\theta)\hat{\jmath} \\
&\quad +((cos^2\Delta\theta - sin^2\Delta\theta - 1)cos\theta_i \\
&\quad +2sin\theta_i sin\phi_i cos\Delta\theta sin\Delta\theta)\hat{k}] \\
&\approx z_0[-(2\Delta\theta)\hat{\jmath} \\
&\quad +(2tan\theta_i sin\phi_i\Delta\theta)\hat{k}] \\
&\approx -2z_0\Delta\theta\hat{\jmath}
\end{aligned}$$

Again, $cos\Delta\theta \approx 1$, $sin\Delta\theta \approx \Delta\theta$ and $sin\theta_i \approx 0$.

Thus, for small angular rotations of the mirror with respect to the transverse axis, the system is linear for transverse displacements produced for a long baseline reflection. For small rotations about the y-axis $\Delta\vec{r}_{r-R} \approx -2z_0\Delta\theta\hat{\imath}$ and about the x-axis $\Delta\vec{r}_{r-P} \approx -2z_0\Delta\theta\hat{\jmath}$. In the linear regime, the optimal angles of incidence for the laser beam is determined as follows

$$|\Delta\vec{r_r}| = \sqrt{|\Delta\vec{r_{r-R}}|^2 + |\Delta\vec{r_{r-P}}|^2} = 2\Delta\theta cos\theta_i$$

and

$$\frac{d|\Delta\vec{r_r}|}{d\theta_i}|_{max} = -2\Delta\theta sin\theta_i \equiv 0$$

Thus, $\theta_i = \{0, n\pi\}$ indicates that the photodiode is most sensitive when aligned near the axis of the mirror.

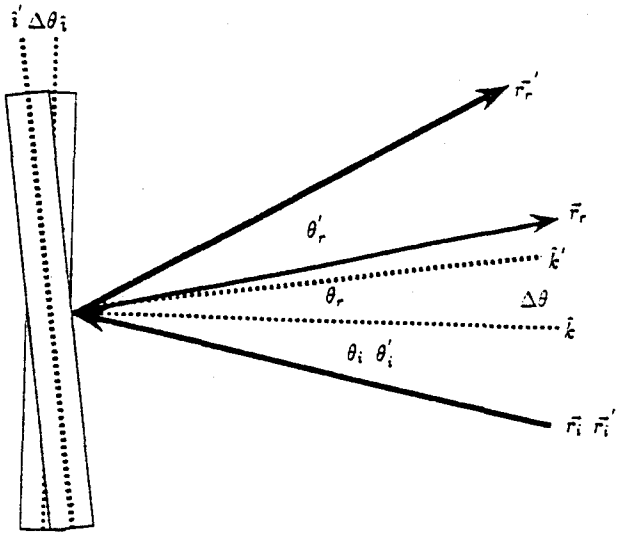

Fig. 10.— The Near Mirror Displacement
The HeNe beam enters delay line from behind a far mirror (not shown) and impinges the center of the near mirror (shown). The reflected light traverses the long baseline giving a large displacement ($\sim z_0 d\theta$) when the light is detected by the photodiode.

4.2. End Mirror

Figure 11 shows the DL configuration as viewed from behind the far mirror. Basically, the residual light from the DL beam (Ar) passes through the mirror and out through a port hole in the end vacuum where it is observed by the photodiode. The present TENKO-100 DL configuration uses L of 96.6 m and mirrors with radius of curvature of 99.5 with the reentrance condition satisfied for 106 total reflections. Under reentrant condition, there are 53 DL beam spots on the far end and 52 on the near the near end, all with varying size depending on the spot number (position). The first beam spot, (x_1, y_1), on the far end is located at 6 o'clock and is the largest, while the second beam spot, (x_3, y_3), on the far end is located at just to the right of 12 o'clock is the second largest, etc. The use of lenses with the photodiode allows the use of very large beam spots and diminishes the effects of intensity and mode changing of the DL laser beam. The final choice of the DL beam spot used, however, is based on the photodiode output and optimum dynamic response for both R and P.

The equations which describe the DL pattern on the mirror are of the following form [Herriot]

$$x_n = x_0 cos(n\theta) + \sqrt{\frac{L}{4f-L}}\left(x_0 + 2f x_0'\right) sin(n\theta)$$
$$y_n = y_0 cos(n\theta) + \sqrt{\frac{L}{4f-L}}\left(y_0 + 2f y_0'\right) sin(n\theta)$$

and

$$(x_0', y_0') = \left(\frac{x_1 - x_0}{L}, \frac{y_1 - y_0}{L}\right)$$

For small angle rotations, the relationship between the transverse displacements, Δx and Δy and the rotation angle can be determined through an interactive process. The first few reflections of the iterative process are shown in Figure 12. Assuming one mirror does not move, the algorithm for determining the n^{th} beam spot position on the rotated mirror, $\Delta\theta$, is summarized as follows:

(1) Reflection Vector - From the given point, $\vec{P_n} = (X_n, Y_n, Z_n)$, and its incident unit-vector,

$$\vec{p_n} = \frac{(X_n, Y_n, Z_n)}{\sqrt{X^2 + Y^2 + Z^2}}$$

, determine the reflection unit-vector at that mirror,

$$\vec{P_{n+1}} = \frac{(X_{n+1}, Y_{n+1}, Z_{n+1})}{\sqrt{X_{n+1}^2 + Y_{n+1}^2 + Z_{n+1}^2}}$$

, using the symmetry wrt. the mirrors radial vector at that point, $\vec{r} = (r_n, r_n, r_n)$, i.e. $\vec{P_n} \cdot \vec{r_n} = \vec{P_{n+1}} \cdot \vec{r_n}$.

(2) Next Point - From the given point, $\vec{P_n} = (X_n, Y_n, Z_n$ and its reflection unit-vector,

$$\vec{P_{n+1}} = \frac{(X_{n+1}, Y_{n+1}, Z_{n+1})}{\sqrt{X_{n+1}^2 + Y_{n+1}^2 + Z_{n+1}^2}}$$

, at one mirror, determine the next point at the other mirror, $\vec{P_{n+1}} = (X_{n+1}, Y_{n+1}, Z_{n+1})$, using the intersection of the mirror plane and the incident (previous reflected) unit-vector,

$$\vec{P_{n+1}} = \frac{(X_{n+1}, Y_{n+1}, Z_{n+1})}{\sqrt{X_{n+1}^2 + Y_{n+1}^2 + Z_{n+1}^2}}$$

This algorithm is used to determine the relationship between small angular rotations of one mirror and the displacement of the DL pattern of that mirror. For the small angular region of interest, Figure 13 (a) shows graphically the linear relationship between the angular rotation and the long baseline transverse

displacement. Shown in (b) of Figure 13 value of this slopes, for a given small angular rotation about the x-axis, versus the different beam spots. This graph of the slopes vs. beam spot location for a small angular rotations about the x-axis, when taken with the same graph of the slopes vs. beam spot location for a small angular rotations about the y-axis, yields an optimal choice of beam spot number n, hence θ. As it turns out the most desirable maximum corresponds to about 25.

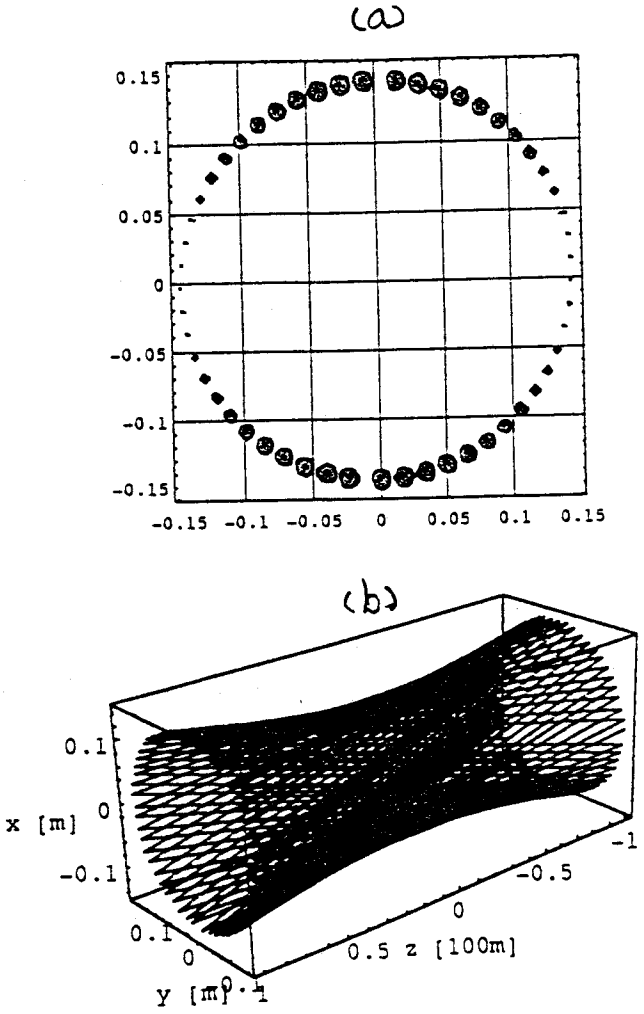

Fig. 11.— The Far Mirror DL Pattern
Shown in (a) is the pattern of the reflected light from the DL (Ar) beam as seen from the front or back of the far mirror. Shown in (b) is a 3-dimensional rendering of the DL pattern produced on the near and the far mirrors in each baseline of the DL interferometer. In practice, the residual DL beam passes through the far mirror and out of the vacuum chamber through a porthole.

It is important to realize that the use of an external laser for an absolute reference in the feedback of the present systems ensures that the near mirror remains stationary. Therefore, the assumption that only one mirror is moving in the derivation of the algorithm is justified. However, in the case where both mirrors have small angular rotations, it is entirely possible to control either mirror from either end of the DL interferometer. Since such a scenario leads to a delay line signal which inherently contains seismic information from the past "folded" into the present, this could result in less than optimal alignment control in the linear regime. The ultimate limit in precision depends on the control component, the feedback control, and inherent frequency cutoff $(3 \times 10^8 \text{m/s}/(106 \times 100)\text{m} \sim 30\text{kHz})$.

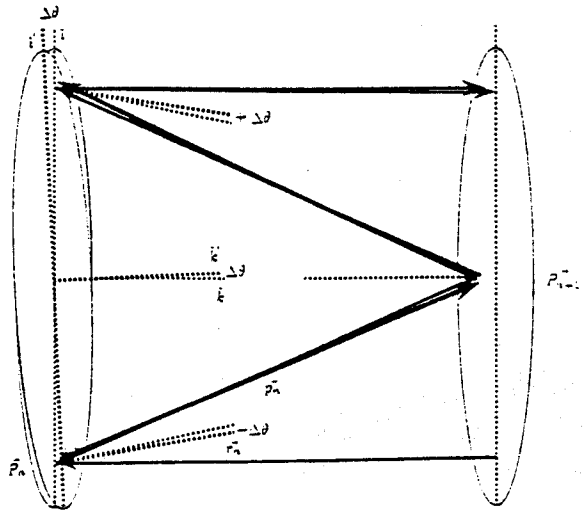

Fig. 12.— The Far Mirror Displacement.
Shown are the first few traces for the laser in application of the angle vs. displacement algorithm. Note in the near mirror case, the normal to the mirror plane and the normal to the mirror surface at the reflection point were the same (center, axis of the mirror), in the far mirror case the two are different.

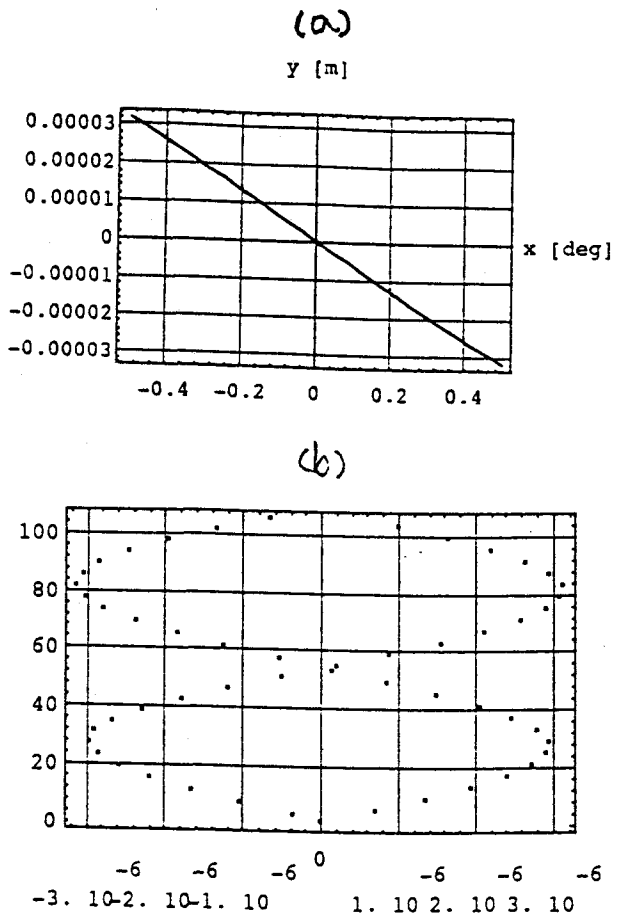

Fig. 13.— The Far Mirror Angle vs. Displacement *Shown in (a) is the angular rotation vs. the transverse displacement for the far mirror. Note the linear behavior over the small angle region of interest for rotational angle vs. displacement Shown in (b) is the slope from angle vs. displacement, i.e. the slope in (a), for different values of n.*

4.3. Linear Control

Since for small angular rotations, the change in the transverse position is linear and with linear gain for the photodiode, the formulation of the feedback control can be understood as a series of linear transformations of information. The first transformation relates the change in roll and pitch, $\Delta R_{\rm in}$ and $\Delta P_{\rm in}$, to the change in the photodiode input signals, $\Delta X(\Delta V_x)$ and $\Delta Y(\Delta V_y)$ via the pre-amplifier gain, g_R and g_P, as follows

$$\begin{pmatrix} \Delta X \\ \Delta Y \end{pmatrix} = \begin{bmatrix} M_{X_r} & 0 \\ 0 & M_{Y_p} \end{bmatrix} \begin{pmatrix} \Delta R \\ \Delta P \end{pmatrix} = \begin{bmatrix} -2z_0\Delta\theta_y g_R & 0 \\ 0 & -2z_0\Delta\theta_x g_P \end{bmatrix} \begin{pmatrix} \Delta R \\ \Delta P \end{pmatrix}$$

Integrating gives,

$$\begin{pmatrix} X \\ Y \end{pmatrix} = \begin{bmatrix} m_{X_r} & m_{X_p} \\ m_{Y_r} & m_{Y_p} \end{bmatrix} \begin{pmatrix} R_{\rm in} \\ P_{\rm in} \end{pmatrix} + \begin{bmatrix} b_{X_r} & b_{X_p} \\ b_{Y_r} & b_{Y_p} \end{bmatrix}$$

Here, the slopes, m, and intercepts, b, can be determined by sweeping the photodiodes in the manner described above. The slopes are found by varying R and P for the mirror control input and measuring, simultaneously, the photodiode response in X and Y. The intercepts roughly correspond to the "origin" of the beam position on the face of the photodiode after manual calibration. These signals serve as the basis for analog filtering and subsequent feedback into the local control of the corresponding optical component.

In the analog approach to feedback control, the signals are filtered, giving rise to a transformation of the signal in terms of phase, $P_X(f)$ and $P_Y(f)$, and gain, $G_X(f)$ and $G_Y(f)$. Hence, the second transformation takes the form,

$$\begin{pmatrix} R_{\rm out} \\ P_{\rm out} \end{pmatrix} = \begin{bmatrix} P_X(f)G_X(f) & 0 \\ 0 & P_Y(f)G_Y(f) \end{bmatrix} \begin{pmatrix} X \\ Y \end{pmatrix}$$

Together, the signal processing in the linear regime is summarized by,

$$\begin{pmatrix} R_{\rm out} \\ P_{\rm out} \end{pmatrix} = \begin{bmatrix} T_X(f) & 0 \\ 0 & T_Y(f) \end{bmatrix} \begin{pmatrix} R_{\rm in} \\ P_{\rm in} \end{pmatrix}$$

where

$$T_X(f) = P_X(f)G_X(f)m_{X_r}$$
$$T_Y(f) = P_Y(f)G_Y(f)m_{Y_p}$$

In practice, implementation of the analog feedback system automatically performs determining the optimum matrix transformation values by the optimization of the filtering in frequency gain and phase.

5. Results

The alignment control system was implemented for the TENKO-100 DL interferometer. The goal in developing and implementing the alignment system was to operate it in standalone mode to reduce the seismic noise of the optical components for the main DL interferometer and to operate it in integrated mode to test for an increase in the data taking time.

In standalone operation, the open-loop system (system off) is shown in (a) of Figure 14 for the frequency domain, while the closed-loop system (system on) is shown in (b) of Figure 14. The closed-loop spectrum shows improvement over the open-loop system from 22 dB to 5 dB in the desired frequency range from 1 to 30 Hz for X (R) and improvement from 25 dB to 2 dB in the desired frequency range from 1 to 30 Hz

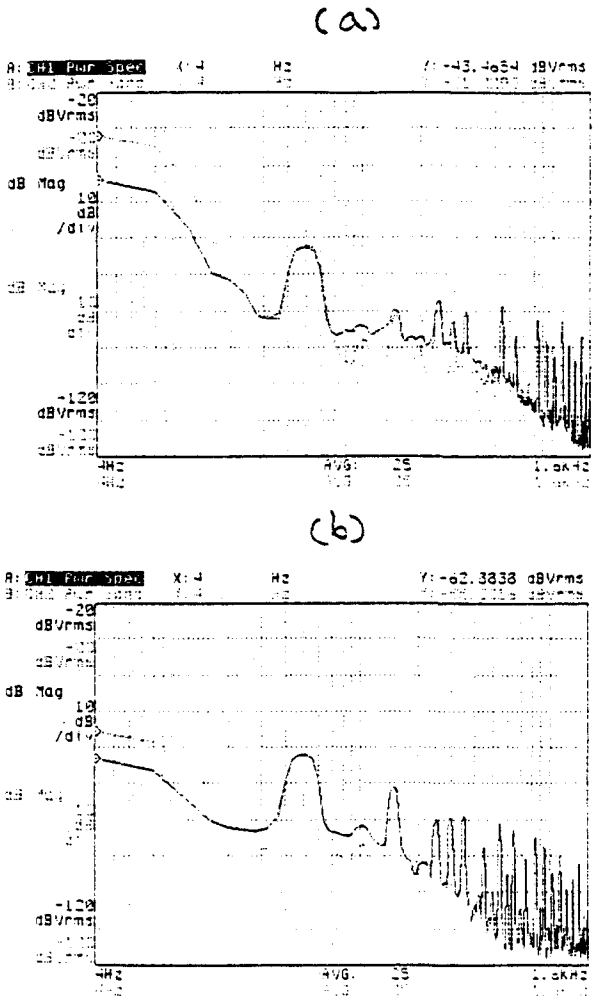

Fig. 14.— Frequency Domain: Power Spectra
Shown in (a) is the open-loop (alignment control off) power spectrum in the frequency domain for one of five optical components of the alignment system, while (b) shows the closed-loop power spectrum (alignment control on) for the same component. Notice, the marked improvement in response in the frequency range of 4 to 30 Hz with the alignment control on.

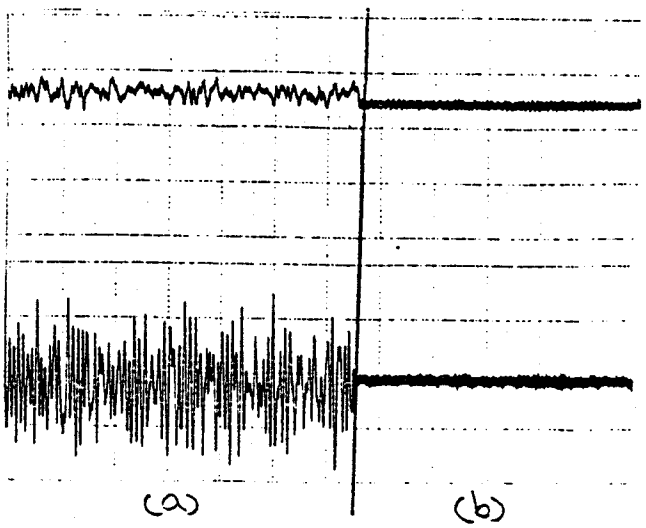

Fig. 15.— Time Domain: Variation Spectra
Shown in (a) is the open-loop (alignment control off) variation spectrum in the time domain for one of the five optical components of the alignment system, while (b) shows the closed-loop (alignment control on) for the same component. Evident is the decrease in the noise amplitude with the alignment control on. The time axis is 1 cm ≡ 12 s and the amplitude axis 1 cm ≡ 10 mV.

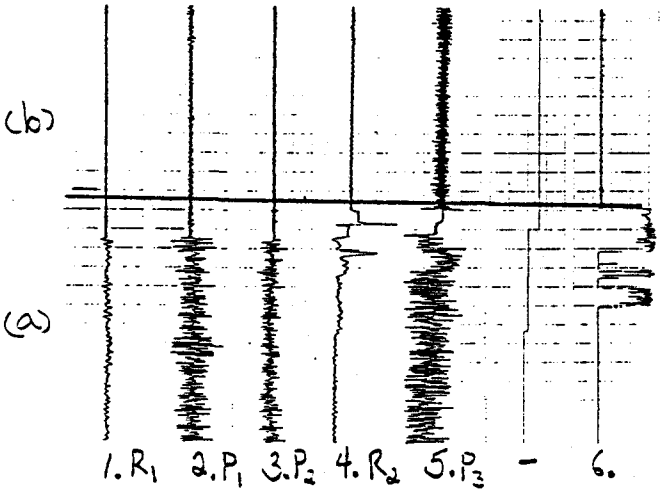

Fig. 16.— Time Domain: Variation Spectra
The variation spectra for output from five of the ten channels contralling the P and R of the five optical components for the alignment system is shown. The sixth channel is the alignment system sensitivity channel output. The integration test demonstrated that the average period of data taking increased from ~ 1 min and ~ 10 min during daytime and nighttime, respectively, without the alignment system to ~ 6 min and ~ 23 min,respectively, with the alignment system.

for Y (P). The time domain spectrum, shown in (a) of Figure 15 for the open-loop system and (b) for the closed-loop system, also indicates effective reduction of the amplitudes for the induced noises from nearby passing cars and trucks. In addition, the standalone system was observed to be very stable over extended periods of time, e.g. $\Delta\tau > 1$ hr.

The results from the integration test of the analog alignment system with all five optical components was performed during both the daytime (noisy) and the nighttime (quiet). Without the alignment system in operation, the average period of data taking (main interferometer dark fringe "locked") was $\sim$ 1 min and $\sim$ 10 min during daytime and nighttime, respectively. WIth the alignment system in operation, the average period of data taking was $\sim$ 6 min and $\sim$ 23 min, respectively. A sample time domain spectrum from the test, shown in Figure 16, also indicates comparable effectiveness in the reduction of the amplitudes for the seismically induced noises.

6. Noises

From the basic flow of information in the system shown in Figure 2, the most prominent areas for noises to occur in the system include the transformation of the reflected laser signal into an electronic signal (shot noise), the amplification of the electronic signal (photodiode pre-amplifier electronic noise), and the signal processing circuit (feedback circuit). The relative noise due to the transformation of the electronic signal into mirror motions (coil actuator) is assumed negligible.

6.1. Electronic Noise

The sources of electronic noise in the system stem from the photodiode pre-amplifier and the feedback circuit. Taken together, the average values of the noise are shown in Table 2, while Figure 17 shows a plot of the noise vs. frequency.

6.2. Shot Noise

Perhaps the most fundamental limit for the system concerns the limit due to the conversion of the reflected laser light into electronic signal, i.e. the shot noise limit. It should be noted that since although the photodiodes for the system are essentially the same, the external laser (HeNe) spot and the DL beam spot are different in terms of total power. The basic shot noise for a photodiode is given as

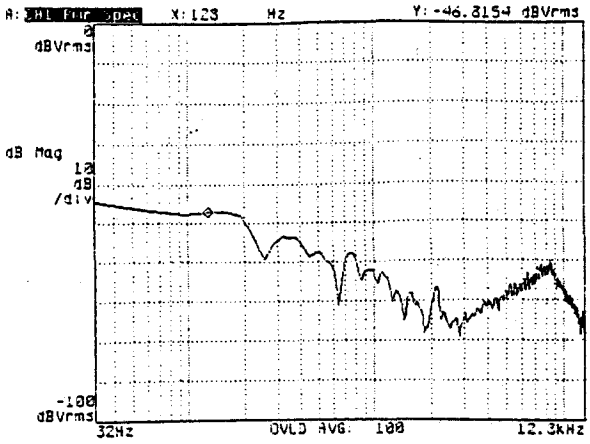

Fig. 17.— The System Electronic Noise
The electronic noise from the pre-amplifier and the feedback circuit is shown. The noise is highest at the lower frequencies and sharply falls off thereafter.

$$\delta L = \sqrt{\frac{\hbar c \lambda}{\pi \eta P}} = \frac{\lambda}{2\pi}\sqrt{\frac{2e}{I}}$$

where h is Planck's constant, c the velocity of light, λ the wavelength of the laser light, P the laser light power, η the quantum efficiency of the photodiode, e the elementary electric charge, and I the photocurrent. Table 2 shows this shot noise limit for the system.

For the actual quadrant photodiodes used, the shot noise limit should be modified according to the geometrical considerations of the detector. Since the output signal is a linear difference of two signals, the shot noise limit should be the addition of these two separate signals, η_+ and η_-, in quadrature. Hence,

Beam	λ [nm]	$< P >$ [mW]	$< \eta_{shot} >$ [m/$\sqrt{\text{Hz}}$]	$< \eta_{elec} >$ [V/$\sqrt{\text{Hz}}$]
HeNe	632.8	1	10^{-15}	5×10^{-7}
DL	514.5	1	10^{-15}	5×10^{-7}

Table 2: Shot Noise and Electronic Noise
The fundamental shot noise and electronic noise measured for the system.

the total shot noise is of the form

$$\eta_{\rm tot} = \sqrt{\eta_+^2 + \eta_-^2}$$

The currents, I_+ and I_-, in each region are proportional to the integration of the laser intensity profile in that region.

7. Conclusion

In summary, an analog alignment control system for TENKO-100 was designed to reduce the instabilities from large transient seismic signals from nearby passing cars and trucks as well as the cumulative effects of background seismic noises. The system was based on the feedback of reflected laser light signals detected with quadrant type photodiodes from each of the five optical components of the main DL interferometer, i.e. four DL mirrors (two near and two far) and one beamsplitter. The alignment system combines the direct use of the main interferometer DL laser light for feedback control of each far mirror and the beamsplitter (relative) and the use of an external laser for feedback control of each near mirror (absolute). Implementation with the TENKO-100 DL interferometer indicate that the system works well in standalone operation for more than one hour during daytime (noisy) operation. The closed-loop (alignment system on) reduction of noise achieved is between 25 to 2 dB in the 1 to 30 Hz range over the open-loop (alignment system off). In integrated tests with the main interferometer high sensitivity locking (data taking mode), the system extended the operating times during the day from $\Delta\tau_{\rm data} \sim 1$ min to ~ 6 min and during the nighttime from $\Delta\tau_{\rm data} \sim 10$ min to ~ 25 min. Improvements for the future will concentrate on reducing the system noises and increasing the operational times of the main interferometer, TENKO-100, in integrated tests. Finally, although the implementation of the system described here is specific to the TENKO-100 DL interferometer, it should not be difficult to adapt such techniques to other DL interferometers as well as Fabry-Perot (FP) type interferometers.

REFERENCES

Weiss, R., *Electromagnetically Coupled Broadband Gravitational Antenna*, RLE Quarterly Progress Report, MIT 105 54 (1972).

Whitcomb, S. *et al.*, *Results from the 40 m Caltech Prototype Gravitational Wave Detector*, Seventh Marcel Grossman Meeting on General Relativity, Stanford Univ. (1994).

Herroit, D. *et al.*, *Off-Axis Paths in Spherical Mirror Interferometers*, Appl Opt. V3 N4 523-526, (1964).

Kawamura, S. *et al.*, *10 m Prototype for the Laser Interferometer Gravitational Wave Antenna*, ISAS Report No. 637, Tokyo, Japan, Sept. 1989.